A TEST OF THE NATURE OF THE FE K LINE IN THE NEUTRON STAR LOW-MASS X-RAY BINARY SERPENS X-1

Chia-Ying Chiang[1], Edward M. Cackett[1], Jon M. Miller[2], Didier Barret[3,4], Andy C. Fabian[5], Antonino D'Aì[6], Michael L. Parker[5], Sudip Bhattacharyya[7], Luciano Burderi[8], Tiziana Di Salvo[9], Elise Egron[10], Jeroen Homan[11], Rosario Iaria[9], Dacheng Lin[12], and M. Coleman Miller[13]

[1] Department of Physics and Astronomy, Wayne State University, 666 W. Hancock, Detroit, MI 48202, USA; ft8320@wayne.edu
[2] Department of Astronomy, The University of Michigan, 500 Church Street, Ann Arbor, MI48109-1046, USA
[3] Universite de Toulouse, UPS-OMP, Toulouse, France
[4] CNRS, Institut de Recherche en Astrophysique et Planetologie, 9 Av. colonel Roche, BP 44346, F-31028 Toulouse cedex 4, France
[5] Institute of Astronomy, University of Cambridge, Madingley Road, Cambridge CB3 0HA, UK
[6] INAF-Istituto di Astrofisica Spaziale e Fisica Cosmica di Palermo, via U. La Malfa 153, I-90146 Palermo, Italy
[7] Department of Astronomy and Astrophysics, Tata Institute of Fundamental Research, Mumbai 400005, India
[8] Dipartimento di Fisica, Università degli Studi di Cagliari, SP Monserrato-Sestu, KM 0.7, I-09042 Monserrato, Italy
[9] Dipartimento di Fisica e Chimica, Universitá di Palermo, via Archirafi 36, I-90123 Palermo, Italy
[10] INAF-Osservatorio Astronomico di Cagliari, via della Scienza 5, I-09047 Selargius (CA), Italy
[11] MIT Kavli Institute for Astrophysics and Space Research, 77 Massachusetts Avenue 37-582D, Cambridge, MA 02139, USA
[12] Space Science Center, University of New Hampshire, Durham, NH 03824, USA
[13] Department of Astronomy and Joint Space-Science Institute, University of Maryland, College Park, MD 20742-2421, USA

ABSTRACT

Broad Fe K emission lines have been widely observed in the X-ray spectra of black hole systems as well as in neutron star systems. The intrinsically narrow Fe K fluorescent line is generally believed to be part of the reflection spectrum originating in an illuminated accretion disk which is broadened by strong relativistic effects. However, the nature of the lines in neutron star low-mass X-ray binaries (LMXBs) has been a matter of debate. We therefore obtained the longest, high-resolution X-ray spectrum of a neutron star LMXB to date with a 300 ks *Chandra* High Energy Transmission Grating Spectrometer (HETGS) observation of Serpens X-1. The observation was taken under the "continuous clocking" mode, and thus was free of photon pile-up effects. We carry out a systematic analysis and find that the blurred reflection model fits the Fe line of Serpens X-1 significantly better than a broad Gaussian component does, implying that the relativistic reflection scenario is much preferred. *Chandra* HETGS also provides a highest spectral resolution view of the Fe K region and we find no strong evidence for additional narrow lines.

Key words: accretion, accretion disks – line: profiles – stars: neutron – X-rays: binaries

1. INTRODUCTION

Broad iron emission lines have been widely discovered in active galactic nuclei (AGNs; Tanaka et al. 1995; Fabian et al. 2009; Brenneman et al. 2011), and in low-mass X-ray binaries (LMXBs) including stellar-mass black holes (Done & Zycki 1999; Miller et al. 2002; Miller 2007; Reis et al. 2009) and neutron stars (NSs; Asai et al. 2000; Barret et al. 2000; Oosterbroek et al. 2001; Di Salvo et al. 2005, 2015; Bhattacharyya & Strohmayer 2007; Iaria et al. 2007; Cackett et al. 2008, 2009a, 2010; Sanna et al. 2013; Pintore et al. 2015). An accretion disk is believed to orbit the central object, and a hard X-ray source, either a power-law continuum or a blackbody component (potentially the "boundary layer"), emits hard X-rays that illuminate the accretion disk. Atomic transitions take place after the high-energy photons are absorbed, which results in a reflection spectrum that includes several narrow emission lines and a broad feature peaked around 20–30 keV which is known as the "Compton hump" (Lightman & White 1988; George & Fabian 1991; Matt et al. 1993; Ross & Fabian 1993, 2005; García & Kallman 2010; Ballantyne et al. 2012).
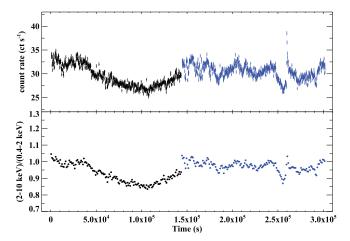
The Fe Kα fluorescent line is the most prominent feature in the reflection spectrum. When appearing in the X-ray spectra of AGNs and LMXBs, the intrinsically narrow Fe lines sometimes show broad, asymmetric profiles which are generally believed to be shaped by a series of relativistic effects induced from strong gravitational fields (Fabian et al. 1989, 2000). As relativistic effects are stronger in the area closer to the compact object, the line profile is sensitive to the inner radius of the accretion disk. If the accretion disk extends to the innermost stable circular orbit (ISCO), then one can, under certain assumptions, obtain an estimate of the black hole spin by measuring the inner radius of the accretion disk (Bardeen et al. 1972). The Fe Kα line profile has been a powerful tool to measure black hole spin (e.g., Miller et al. 2002; Reynolds & Nowak 2003; Brenneman & Reynolds 2006; Miller 2007; Reis et al. 2008, 2012). The inner radius of the accretion disk in a NS system can be determined using the same method. The accretion disk in an NS system could be truncated by the stellar surface or the boundary layer between the disk and the NS, if the NS is larger than its ISCO, or by a strong stellar magnetic field. An upper limit of the stellar radius of an NS can be given by measuring the inner radius of the disk, and hence can help us to understand its equation of state (e.g., Piraino et al. 2000; Cackett et al. 2008). Bhattacharyya (2011) reported more detailed calculations to show how future instruments can directly constrain NS equation of state models using relativistic disk lines.

In NS systems, the Fe Kα lines are usually not as prominent (EW ∼ 100 eV) as those seen in AGNs and black hole binaries (BHBs) due to extra continuum emission from the boundary

layer. It has been widely accepted that relativistic Fe K lines are common in AGNs (Reynolds & Nowak 2003) and BHBs (Miller 2007), although some suggest that line profiles could be caused by warm absorbers (Inoue & Matsumoto 2003) or Comptonization (Laurent & Titarchuk 2007). Nonetheless, whether Fe K lines in NS systems are relativistically broadened is still under debate. Ng et al. (2010) analyzed a number of *XMM-Newton* NS spectra and concluded that statistical evidence of asymmetric iron line profiles is lacking and the lines are broadened by Compton scattering in a disk corona (Misra & Kembhavi 1998; Misra & Sutaria 1999). Reynolds & Wilms (2000) showed that the continuum source required in the Compton scattering model to produce the broad iron line violates the blackbody limit. Although the calculation was based on the AGN case, small radii of the Compton clouds are still required to maintain the high ionization level in NS systems, which would make gravitational effects dominant (Fabian et al. 1995). Furthermore, the pile-up correction applied in Ng et al. (2010) reduced the signal-to-noise ratio of the data and made it difficult to detect relativistic iron lines (see Figure 2 in Miller et al. 2010). Cackett et al. (2010) examined a large sample of *Suzaku* NS spectra and found that the relativistic reflection scenario is much preferred. The iron line detections with *Suzaku* are less affected by photon pile-up effects than those of *XMM-Newton*, and thus the conclusion that iron lines are asymmetric is likely more robust. A study of the effects of pile-up in X-ray CCD detectors by Miller et al. (2010) showed that while pile-up can distort the Fe K line profiles, it tends to artificially narrow them (in contrast with the findings of Ng et al. 2010).

Detections made with spectrometers that suffer no photon pile-up effects become important when determining the iron line profiles. The re-analyses of archival *BeppoSAX* data of 4U 1705–44 implied the existence of asymmetric Fe K lines (Piraino et al. 2007; Lin et al. 2010; Cackett et al. 2012; Egron et al. 2013). *NuSTAR* sees an asymmetric line in Serpens X-1 (Miller et al. 2013) with line properties consistent with the *Suzaku* measurements from Cackett et al. (2008, 2010, 2012). The pile-up free detectors *BeppoSAX* and *NuSTAR* both reach the conclusion of relativistic iron lines. These instruments are, however, not capable of detecting possible narrow line components on top of the broad Fe K lines. So far, the *Chandra* High Energy Transmission Grating Spectrometer (HETGS) is the only instrument that offers a pile-up free observation at high spectral resolution (approximate $\Delta E \sim 30$ eV at 6 keV).

The neutron star LXMB Serpens X-1 was discovered in 1965 (Friedman et al. 1967). Being a persistent, bright X-ray source, Serpens X-1 has been observed with major X-ray missions including *Einstein* (Vrtilek et al. 1986), *ASCA* (Asai et al. 2000), *EXOSAT* (Seon & Min 2002), *BeppoSAX* (Oosterbroek et al. 2001), *INTEGRAL* (Masetti et al. 2004), *XMM-Newton* (Bhattacharyya & Strohmayer 2007), *Suzaku* (Cackett et al. 2008, 2010), and recently with *NuSTAR* (Miller et al. 2013). It was also detected in the optical (Hynes et al. 2004) and radio (Migliari et al. 2004) bands. Relativistic Fe K lines have been reported several times in previous *Suzaku*, *XMM-Newton*, and *NuSTAR* observations (Bhattacharyya & Strohmayer 2007; Cackett et al. 2008, 2010; Miller et al. 2013). In this paper, we study the latest high-resolution *Chandra* HETGS observation, which is the longest *Chandra* grating observation of a neutron star LMXB to date. We present

Figure 1. Upper panel: the 0.4–10 keV light curve of Serpens X-1. The light curve was extracted from the first-order HEG data. The gap between the observations has been discarded. Black points stand for data extracted from the first half of the observation, and blue ones for the second. There is a weak type I X-ray burst containing ∼0.5% of the total counts in the second half of the observation. Lower panel: the hardness ratio, which is the hard (2–10 keV) light curve divided by the soft (0.4–2.0 keV) light curve.

detailed data analysis and results in the following sections. The Galactic absorption column N_H is assumed to be 4.4×10^{21} cm^{-2} (Dickey & Lockman 1990) with "wilm" abundances (Wilms et al. 2000) throughout all of our analyses, which were performed using the XSPEC 12.8.2 package (Arnaud 1996). All of the errors quoted in the paper are given at the 90% confidence level.

2. DATA REDUCTION

Serpens X-1 was observed with the *Chandra* HETGS during 2014 June 27–29 and August 25–26 (Obs. ID: 16208, 16209), providing a total good exposure of ∼300 ks. The observation was taken using the "continuous clocking (CC)" mode. We reduced the data following the standard procedures using the latest CIAO V4.6 software package. The CC mode provides 2.85 ms time resolution, and hence the observation is clear of photon pile-up effects and has negligible background. In this work, we concentrate on the HEG (high-energy grating) data which cover the Fe line energy band. We found the HEG $+1$ and -1 spectra to differ at the 5%–10% level, especially around the area of a chip gap in the $+1$ spectrum. Thus, we tested a number of methods to improve the $+1$ spectrum (see Appendix). However, the discrepancy cannot be completely eliminated, and thus we only use the HEG -1 spectrum in this work.

The spectra of each observation from 2014 June and August are similar and we combined them to form a long spectrum. All of the spectral bins from 2 to 8 keV have more than 30 counts per bin, and thus no rebinning is required. We found a number of wiggles in the spectrum below 2 keV that could not be modeled. Their locations matched the locations of significant sharp changes in the effective area. We therefore use the 2.0–8.0 keV energy band in the following analysis. A restricted energy band is often used for the data taken under the CC mode to avoid artificial instrumental artifacts (e.g., Cackett et al. 2009b; Miller et al. 2011, 2012; Degenaar et al. 2014).

The upper panel of Figure 1 displays the 0.4–10.0 keV light curves of Serpens X-1 during the observation. It can be seen that there is a weak type I X-ray burst, which originates from

the thermonuclear burning of matter on the NS surface (Woosley & Taam 1976; Lamb & Lamb 1978; Strohmayer & Bildsten 2006), in the later observation (shown in blue data points). The X-ray burst lasted for a few hundreds of seconds and contributed $\sim 4.7 \times 10^4$ counts, which is only $\sim 0.5\%$ of the total $\sim 8.9 \times 10^6$ counts of the entire observation. Since the burst is such a small fraction of the total counts and casts no effects on the spectrum, we did not exclude the data during the X-ray burst.

3. DATA ANALYSIS

3.1. Continuum

Continuum models for NS LMXBs can be degenerate, at least over narrow wavelength ranges, as we have here. They can be equally well explained by different continuum models consisting of a disk blackbody, a blackbody-like component (to fit the boundary layer emission), and a power-law or Comptonized component (e.g., Barret 2001; Lin et al. 2007). We test three different continuum models, which are a disk blackbody plus a blackbody (Model 1), a disk blackbody plus a power-law (Model 2), and a blackbody plus a power-law (Model 3), in order to determine the necessary spectral components required to interpret the spectrum of Serpens X-1 in this observation. As mentioned in Section 2, we use HEG -1 over the 2.0–8.0 keV energy band. The Galactic absorption is modeled by TBABS in XSPEC, the accretion disk blackbody emission by DISKBB, and the thermal emission from the NS boundary layer by BBODY.

An iron emission line has been clearly detected in the HEG -1 spectrum, and we start by modeling the feature with a Gaussian line (GAUSSIAN in XSPEC). In all of our fits, we restrict the line energy to be in the range of 6.4–6.97 keV where neutral/ionized iron Kα lines can only appear. However, given the relatively narrow energy range of the continuum, we find that the width (σ) of the Gaussian tends to have large values (1–1.5 keV), and large normalizations giving equivalent widths (EWs) greater than 500 eV, even when fixing the energy of the line to 6.4, 6.7, or 6.97 keV. Since this is not seen in neutron star LMXB spectra, we restrict the width of the Gaussian based on previous fits to Serpens X-1. For instance, the broadest width that Ng et al. (2010) obtain when fitting a Gaussian to the *XMM* data of Serpens X-1 is $\sigma = 0.27^{+0.14}_{-0.11}$ keV. Fits to other archival spectra of Ser X-1 tend to provide slightly broader Gaussians than this. For instance, by averaging all of the fits in Cackett et al. (2012), we find an average Gaussian width of $\sigma = 0.61$ keV. Using these as a guide, we try spectral fits with (a) σ restricted to be less than the upper limit of 0.41 keV from Ng et al. and (b) σ restricted to be less than 0.61 keV from Cackett et al. (2012).

Including a broad Gaussian component in the iron line energy band significantly improves the fit (the smallest improvement was $\Delta\chi^2 \sim 150$ lower with three fewer degrees of freedom (dof)), confirming the clear detection of the broad iron emission line (also see differences between model residuals in Figure 2). In Table 1, we show the fitting results of the three possible continuum models. Note that we also tried fitting with all three continuum components, but found that the power-law index became unconstrained in those fits.

Models 1b and 2a–b give comparable quality fits, however, they all result in unphysical parameters. In Model 1b, when a larger σ is allowed than in Model 1a, we obtain an unusually
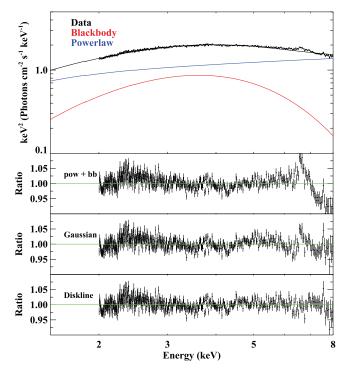

Figure 2. Top panel: the unfolded spectrum of Serpens X-1 with decomposed model components. We display the data/model ratios of the continuum model `tbabs*(bbody + power-law)` Model 3, and Model 3a in the lower panels.

high blackbody temperature (see Table 1). Furthermore, when replacing the Gaussian with a DISKLINE, we get an unphysical blackbody temperature (>5 keV), which is insensitive to the data (the peak of the blackbody is well outside of the HEG energy range). The typical blackbody temperature seen in NS systems is generally below ~ 2.5 keV (Lin et al. 2010, 2012; Piraino et al. 2012; Di Salvo et al. 2015). In Models 2a–b, the photon indices for the power-law are very hard ($\Gamma = 0.94$), which is also unexpected as the photon indices of NSs usually fall within the 1.5–3.0 range (Cackett et al. 2010, 2012; Egron et al. 2013; Di Salvo et al. 2015). Therefore, while Models 3a–b do not give the best fit statistically, we use those models for the continuum in the following analysis.

It is interesting to note that both Models 1a and 1b fit equally well, yet have quite different Gaussian widths. This can be viewed as evidence that the broad line is asymmetric, since a relativistic line with a narrow core and broad red wing can be well fit by two Gaussians—one reasonably narrow and one broad (Cackett et al. 2008, 2012). Fits with two Gaussians to *Suzaku* spectra of Ser X-1 yield widths of 0.14 keV and 0.64 keV (Cackett et al. 2012), which are comparable to the widths in Models 1a and 1b.

3.2. Iron Line

An iron emission line was clearly detected in the spectrum, implying that a reflection component is present in the system. The iron line of Serpens X-1 seems to extend for at least 1 keV, indicating possible signatures of relativistic effects similar to those seen in stellar-mass black holes and AGNs. We test the nature of the line by fitting several different models. If the line is broadened by relativistic effects, then it should be better fit by a relativistic line model rather than a broad Gaussian. Given the high spectral resolution of the *Chandra* HEG, we also have

Table 1
Best-fitting Parameters for Different Continuum Models

Component	Parameter	Model 1a	Model 1b	Model 2a	Model 2b	Model 3a	Model 3b
TBABS	N_H (10^{22} cm^{-2})	(0.44)	(0.44)	(0.44)	(0.44)	(0.44)	(0.44)
DISKBB	kT_{disk} (keV)	$1.34^{+0.05}_{-0.03}$	1.42 ± 0.04	1.42 ± 0.01	$1.44^{+0.01}_{-0.02}$	...	...
	N_{disk}	$80.0^{+6.8}_{-8.3}$	$68.3^{+6.5}_{-3.4}$	$60.1^{+2.3}_{-3.0}$	$61.7^{+1.4}_{-2.8}$	...	...
BBODY	kT_{bb} (keV)	$2.39^{+0.33}_{-0.19}$	$2.90^{+0.82}_{-0.44}$	...	...	$0.90^{+0.20}_{-0.17}$	$0.90^{+0.02}_{-0.01}$
	N_{bb} (10^{-2})	2.6 ± 0.1	$2.5^{+0.5}_{-0.2}$	...	...	2.3 ± 0.1	2.4 ± 0.1
POWERLAW	Γ	...	...	$0.94^{+0.28}_{-0.12}$	$0.68^{+0.29}_{-0.35}$	1.78 ± 0.02	1.80 ± 0.02
	N_{pow}	...	...	0.10 ± 0.04	$0.05^{+0.05}_{-0.03}$	0.88 ± 0.03	$0.87^{+0.03}_{-0.02}$
GAUSSIAN	E_{line} (keV)	$6.62^{+0.04}_{-0.13}$	$6.48^{+0.09}_{-0.06}$	$6.52^{+0.05}_{-0.07}$	$6.43^{+0.05}_{-0.03}$	$6.43^{+0.05}_{-0.03}$	$6.40^{+0.02}$
	σ (keV)	$0.26^{+0.15}_{-0.06}$	$0.61_{-0.11}$	$0.41_{-0.03}$	$0.61_{-0.03}$	$0.41_{-0.01}$	$0.61_{-0.02}$
	N_{gau} (10^{-3})	$1.9^{+1.1}_{-0.5}$	$4.6^{+0.6}_{-1.4}$	$3.1^{+0.3}_{-0.4}$	5.0 ± 0.6	$3.1^{+0.3}_{-0.4}$	5.3 ± 0.6
	EW (eV)	48^{+11}_{-10}	115^{+42}_{40}	76^{+20}_{-16}	123^{+75}_{-29}	74^{+16}_{-14}	128^{+41}_{-35}
χ^2/dof		2052/1852	2051/1852	2072/1852	2056/1852	2184/1852	2148/1852

Note. Models 1a/1b includes both DISKBB and BBODY components; Models 2a/2b are composed of DISKBB and the power-law continuum; Models 3a/3b are comprised of BBODY and power-law components. Both Model 3a and Model 3b gave most reasonable fitting parameters.

Table 2
Best-fitting Spectral Parameters Testing Different Models for the Fe K Emission Line

Component	Parameter	Model 3b	Model 4a	Model 4b	Model 4c
TBABS	N_H (10^{22} cm^{-2})	(0.44)	(0.44)	(0.44)	(0.44)
BBODY	kT_{bb} (keV)	$0.90^{+0.02}_{-0.01}$	$0.89^{+0.01}_{-0.02}$	0.89 ± 0.01	0.90 ± 0.01
	N_{bb} (10^{-2})	2.4 ± 0.1	2.4 ± 0.1	2.2 ± 0.1	2.3 ± 0.1
POWERLAW	Γ	1.80 ± 0.02	1.74 ± 0.02	1.75 ± 0.02	1.78 ± 0.01
	N_{pow}	$0.87^{+0.03}_{-0.02}$	$0.81^{+0.03}_{-0.02}$	$0.88^{+0.02}_{-0.03}$	0.88 ± 0.01
GAUSS 1 (broad)	E_{line1}	$6.40^{+0.02}$	...	...	$6.4^{+0.03}$
	σ (keV)	$0.61_{-0.02}$	...	...	$0.41_{-0.01}$
	N_{gau} (10^{-3})	5.3 ± 0.6	...	...	2.7 ± 0.3
	EW (eV)	128^{+41}_{-35}	...	...	64^{+16}_{-14}
GAUSS 2 (width $= 0$)	E_{line2}	...	...	6.57 ± 0.01	6.57 ± 0.01
	N_{gau} (10^{-4})	...	...	$2.1^{+0.6}_{-0.4}$	1.4 ± 0.5
	EW (eV)	...	...	5^{+2}_{-1}	3^{+2}_{-1}
GAUSS 3 (width $= 0$)	E_{line3}	...	...	6.67 ± 0.01	6.67 ± 0.01
	N_{gau} (10^{-4})	...	...	$1.8^{+0.5}_{-0.4}$	1.2 ± 0.5
	EW (eV)	...	...	5^{+1}_{-2}	3 ± 1
DISKLINE	E_{line} (keV)	...	$6.97_{-0.02}$	...	...
	q	...	$5.65^{+0.51}_{-0.43}$	...	...
	R_{in} (RM/c^2)	...	7.7 ± 0.1	...	...
	inclination	...	24 ± 1	...	...
	$N_{diskline}$ (10^{-3})	...	5.8 ± 0.5	...	...
	EW (eV)	...	149 ± 15	...	...
χ^2/dof		2148/1852	2015/1850	2286/1851	2149/1848

Note. Model 4a tests a relativistic line, while Models 4b tests narrow lines only and 4c tests a combination of a broad Gaussian and narrow lines. The relativistic line model is by far the best fit. Note that the definition of emissivity index β in the DISKLINE model is $\epsilon(r) = r^{\beta}$ (where r is the disk radius) instead of $\epsilon(r) = r^{-q}$, and here we quote q, which is equal to $-\beta$.

the opportunity to test whether there are any narrow line components that contribute to the line shape that are otherwise unresolved with other detectors.

First, we tested the relativistic reflection model by fitting the Fe emission line using the DISKLINE (Fabian et al. 1989) model in XSPEC. We replaced the broad Gaussian component in Models 3a/3b with DISKLINE to build a new model (hereafter Model 4a). See Table 2 for the best-fitting values. This model fits significantly better than a broad Gaussian, with an improvement of $\Delta\chi^2 = 133$ for two more dof.

We find an inner disk radius of $7.7 \pm 0.1\,R_G$ (where $R_G = GM/c^2$) and an inclination of $24° \pm 1°$. We show the iron line profile and the best-fitting DISKLINE model in Figure 3. The DISKLINE component clearly fits the Fe line very well. Other relativistic line models such as LAOR and RELLINE were also tested, and all of them fit the Fe line as well as DISKLINE does, with similar parameters. Note that if we use Models 1a/1b for the continuum instead of Models 3a/3b, then we get consistent DISKLINE parameters and a large improvement in χ^2 ($\Delta\chi^2 \sim 72$–73), although due to the
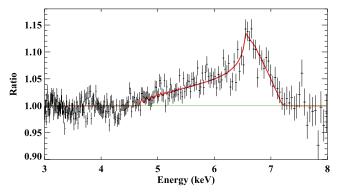
Figure 3. Fe line profile of Serpens X-1. The spectrum is modeled as `tbabs` `(bbody + power-law + diskline)`, and the plot is produced by setting the normalization of DISKLINE to be 0. The plot is visually binned with "septplot rebin" in XSPEC. The bin sizes through the Fe line are ~0.042 keV. The red line shows model. It can been seen that the DISKLINE model fits the asymmetric line very well.
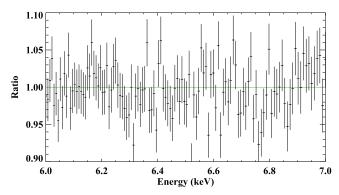

Figure 4. The 6.0–7.0 keV data/model ratio fit using the DISKLINE model. The data are unbinned with bin sizes of ~0.008 keV. It can be seen that no obvious emission or absorption features presenting in the figure.

narrow energy range we get a high blackbody temperature which is unconstrained.

Next, we tested whether or not the line could be fitted by two narrow Gaussian components (Model 4b). The line width σ of each narrow Gaussian component was set to be zero. Model 4b provides a significantly worse fit than Model 3b, indicating that narrow lines alone cannot fit the data. We next tested for the presence of narrow lines in addition to a broad component (Model 4c), which gave a comparable fit than Model 3b, but a significantly worse fit than the relativistic line ($\Delta\chi^2 = 134$ higher, with two fewer dof). A model including three narrow lines was tested but did not improve the fit. We also tried to set the line energies of the narrow Gaussian components to be those of the Fe XXV (6.67 keV) and Fe XXVI (6.97 keV) lines, and again this did not yield a better fit. The equivalent widths of the narrow Gaussian lines in Models 4b and 4c are all small (EW ~ 3–5 eV). We also tested using narrow Gaussian components with physical upper limits of the line widths as well. Assuming a narrow line originates from the outer part of the accretion disk and is broadened by thermal effects in a ~10^7 K gas, the line width should be $\sigma \lesssim 0.007$ keV. This again made no improvement in the fit. From the series of tests, we conclude that there is no strong evidence of narrow emission lines. We present the detailed 6.0–7.0 keV data/model ratio in the lower panel of Figure 4. It can be clearly seen that Model 4a fits this band very well and no obvious emission or absorption features are present.

In conclusion, of all the models with which we tried to fit the Fe K line in Serpens X-1, we find that a relativistic line model fits significantly better than any others, which indicates that the Fe line profile is caused by relativistic broadening and no narrow line components are required to explain the spectrum. The result acts to validate the relativistic reflection scenario.

3.3. Relativistic Reflection Model

As the Fe emission line is best interpreted by the relativistic reflection scenario, we replace the DISKLINE component in Model 4a with a blurred broadband reflection model. The reflection model self-consistently accounts for not only the Fe K line, but other lines and continuum emission expected due to reflection and broadening due to Comptonization based on the ionization parameter. The reflection model is then blurred by relativistic effects.

Table 3
Fitting Results of the Relativistic Reflection Models

Component	Parameter	REFLIONX	XILLVER
TBABS	$N_{\rm H}$	(0.44)	(0.44)
BBODY	$kT_{\rm bb}$ (keV)	0.86 ± 0.01	0.87 ± 0.01
	$N_{\rm bb}$ (10^{-2})	2.7 ± 0.1	2.6 ± 0.1
POWERLAW	Γ	1.68 ± 0.03	1.75 ± 0.03
	$N_{\rm pow}$	0.56 ± 0.06	$0.73^{+0.02}_{-0.04}$
KDBLUR	q	$5.1^{+1.8}_{-1.0}$	$4.4^{+1.1}_{-0.7}$
	$R_{\rm in}$ ($R_{\rm G}$)	$7.1^{+1.1}_{-0.6}$	$8.4^{+1.1}_{-0.2}$
	i (deg)	29 ± 1	33 ± 1
REFLECTION	$A_{\rm Fe}$	$1.00^{+0.56}_{-0.11}$	$1.52^{+1.47}_{-0.60}$
	ξ	270^{+80}_{-30}	130^{+70}_{-30}
	$N_{\rm ref}$	$6.8^{+2.0}_{-2.3} \times 10^{-5}$	$0.19^{+0.64}_{-0.15}$
χ^2/dof		1968/1849	2012/1848

Note. It can be seen that REFLIONX and XILLVER yield similar parameters.

In NS systems, the accretion disk may be illuminated by the thermal emission coming from the boundary layer of the NS or by a power-law continuum, resulting in reflected emission (Cackett et al. 2010; D'Aì et al. 2010). The continuum of Serpens X-1 in this observation is dominated by the power-law component, and we use the REFLIONX model (Ross & Fabian 2005), which calculates the broadband reflection spectrum from the accretion disk illuminated by a power-law continuum. The convolution model we use to account for relativistic effects is the KDBLUR kernel. We assumed the outer radius to be 400 $R_{\rm G}$. The iron abundance $A_{\rm Fe}$ was set to vary in the range between 1 and 4 times the solar value. The model fits the spectrum well, and we report the best-fitting parameters in Table 3. The values of the inner radius $R_{\rm in}$ and inclination angle i we obtained are very similar to those given by Model 4a. The model using REFLIONX yielded a better fit than Model 4a ($\Delta\chi^2 \sim 50$ lower with one fewer dof).

We also tested the XILLVER reflection model (García & Kallman 2010; García et al. 2013). While the fit using XILLVER yielded a worse fit than that using the REFLIONX grid, the best-fitting parameters are comparable to those of Model 4a. In Table 3, it can be seen that models using different reflection grids gave consistent results. The parameters of KDBLUR obtained from both models are fairly similar, and both gave a inner radius of $R_{\rm in} \sim 7-8\ R_{\rm G}$ and a low inclination angle ($i \sim 30$).

4. DISCUSSION

We analyzed a 300 ks *Chandra*/HEG observation of the NS LMXB Serpens X-1. We fit a number of models to the 2–8 keV HEG −1 spectrum to examine the nature of the Fe emission line, and we find that the origin of the line is best explained by relativistically broadened reflection. Fitting broadband reflection models implies an inner radius of ∼7–8 R_G and a low inclination of $i \sim 25°$–$35°$. In the following subsections, we discuss the robustness of the line parameters and compare our results with previous results in the literature.
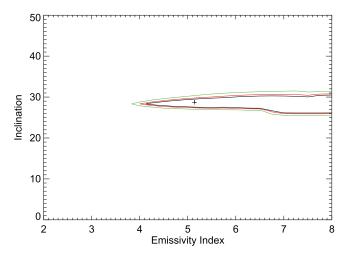
4.1. Choice of Continuum Model

It is difficult to constrain the continuum using a restricted 2–8 keV energy band, and so we choose the model with the most reasonable fitting parameters (a blackbody and a power-law) to be the continuum in this work. In fact, Serpens X-1 has only been observed in the soft state, and the power-law component is usually weak. To explain the spectrum of an NS in the soft state, then a continuum composed of a disk blackbody component contributed by the accretion disk and a blackbody component possibly caused by the thermal emission from the boundary layer (Model 1a/1b) is more likely. If we replace the Gaussian component with the DISKLINE model in Models 1a/1b and re-fit the spectrum, we still obtain DISKLINE parameters similar to those of Model 4a ($E_{line} = 6.93 \pm 0.04$ keV; emissivity index $= -5.2^{+0.5}_{-0.3}$; $R_{in} = 7.2 \pm 0.1\,R_G$; $i = 26° \pm 1°$). We also conduct the same test on Models 2a/2b and find that the choice of continuum does not affect the parameters of the DISKLINE component.

Assuming that the continuum of Serpens X-1 is soft and dominated by the thermal emission from the boundary layer, the illuminating source is then the blackbody component. In order to further test the broadband relativistic reflection model with a soft continuum (disk blackbody plus blackbody), we use the BBREFL grid (Ballantyne 2004; reflection calculated assuming a blackbody component to illuminate the accretion disk) instead of REFLIONX to account for reflection. The model composed of a soft continuum and relativistic reflection (KDBLUR*BBREFL) provides the best-fitting inner radius $R_{in} = 8.1^{+0.7}_{-1.2}\,R_G$ and inclination angle $i = 34^{+1}_{-3}°$, which are consistent with those obtained using a harder continuum with the REFLIONX/XILLVER grids.

4.2. No Additional Narrow Line Components

In Section 3.2, we test various models to fit the Fe K line and show that the line can simply be fit by a relativistically broadened reflection component. Given the unique spectral resolution of *Chandra* HETGS, we have the opportunity to test for the presence of any narrow lines in addition to the broad line. We find that including narrow lines in addition to a broad Gaussian gives a worse fit than the relativistic line alone. We include narrow Gaussian components with reasonable line energies (6.4, 6.67, and 6.97 keV) to Model 4a and the broadband relativistic reflection models to examine the existence of narrow lines. Narrow components at 6.4 and 6.67 keV do not improve the fit of Model 4a, while the narrow Gaussian line at 6.97 keV improves the fit marginally ($\Delta\chi^2 \sim 3$ lower than Model 4a). The narrow lines at 6.67 keV and 6.97 keV improve the fit of the REFLIONX model marginally ($\Delta\chi^2 \sim 5$–10 lower than the REFLIONX model), but the equivalent widths of these lines are low

Figure 5. Contour plot of the emissivity index against the inclination angle, which was calculated from the REFLIONX model. The contours are plotted at 67% (black), 90% (red), and 99% (green) confidence levels. It can be seen that there is no clear degeneracy between emissivity and inclination angle.

(EW ∼ 2 eV). Furthermore, examination of Figure 4 shows no evidence for narrow lines in the residuals of the relativistic line fit. Hence, we conclude that there is no strong evidence of narrow components.

4.3. Comparison with Previous Work

Bhattacharyya & Strohmayer (2007), Cackett et al. (2010), and Miller et al. (2013) reported the existence of relativistic Fe K lines in Serpens X-1 using *XMM-Newton*, *Suzaku*, and *NuSTAR* data, respectively. In Bhattacharyya & Strohmayer (2007), the continuum was modeled as an absorbed Comptonization (compTT) plus a disk blackbody, while in the latter two pieces of work a full continuum (a disk blackbody, a blackbody plus a power-law) was used. Bhattacharyya & Strohmayer (2007) used the LAOR model to fit the Fe K line, while Cackett et al. (2010) and Miller et al. (2013) used the blurred BBREFL and REFLIONX models to account for relativistic reflection. Bhattacharyya & Strohmayer (2007) obtained an inclination angle of $i \sim 40°$–$50°$, which is higher than the best-fitting values of Cackett et al. (2010; $i \lesssim 25°$) and Miller et al. (2013; $i \lesssim 20°$) and this work ($i \sim 30°$). Cackett et al. (2010) also analyzed the same *XMM-Newton* data set used in Bhattacharyya & Strohmayer (2007) and found that low inclination ($i \lesssim 30°$) is preferred.

Cackett et al. (2010) and Miller et al. (2013) both obtained a low emissivity index of $q \sim 2.3$, while a higher value of $q \sim 4$–5 is required in this work. We note that inclination and emissivity can be degenerate (see Figure 8 in Cackett et al. 2010), but such a degeneracy was not found in this work (see Figure 5). The emissivity index depends on the Fe K line profile and it is likely that the line profile is slightly different from those of previous observations due to the better spectral resolution of *Chandra* grating data in this energy band. Regardless, our fits suggest a small inner radius, which is consistent with previous findings. In this work, the broad iron line profile implies an inner radius of ∼7–8 R_G. Previous analyses on *XMM-Newton*, *Suzaku*, and *NuSTAR* data suggest the inner radius to be ∼4–25 R_G, ∼6–8 R_G, and ∼6–8.5 R_G, respectively. The *XMM-Newton* observation was taken under timing mode with a short exposure time, which causes some uncertainties in constraining parameters. The later *Suzaku*,
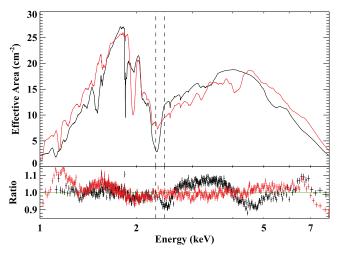
NuSTAR, and current observations all give well-constrained parameters, which is consistent with measurements of the inner radius. Although different continuum models were used to fit the spectra of Serpens X-1 observed with various instruments at different times/fluxes, previous and current analyses all indicate that the source has a low inclination angle and small inner radius.

All of the previous observations of Serpens X-1 discussed above place the inner disk radius close to the ISCO. When compared to the broader class of NS LMXBs, most other sources have an inner disk radius consistent with ISCO, regardless of source luminosity (for instance, see Figure 7 of Cackett et al. 2010, for a comparison over two orders of magnitude in luminosity). Clear exceptions to this are SAX J1808.4–3658 (Cackett et al. 2009a; Papitto et al. 2009), IGR J170480–2446 (Miller et al. 2011), and GRO J1744–28 (Degenaar et al. 2014), all of which are pulsars whose magnetic field must truncate the inner accretion flow. In low/hard states, accretion flow models suggest that the disk should recess, being replaced by a hot, radiatively inefficient flow (see, e.g., Done et al. 2007, for a review). However, iron line studies of NS LXMBs in low states do not show large disk truncation. For instance, a *NuSTAR* observation of 4U 1608-52 at 1%–2% of the Eddington limit has a disk that extends close to ISCO (Degenaar et al. 2015), while broadband *Suzaku* observations of 4U 1705–44 at 3% Eddington also show that the disk is not truncated at large radii (Di Salvo et al. 2015). Thus, the majority of NS LMXBs, including Serpens X-1, show inner disk radii that are close to ISCO, with no strong dependence on state or luminosity.

5. CONCLUSION

We analyze the latest long HETGS data of Serpens X-1 and examine the nature of its Fe emission line. A thermal blackbody component, possibly contributed by the boundary layer of the NS, and a power-law component provide a good fit to the continuum without unphysical parameters. By studying the Fe emission line in the spectrum, we find that the relativistic reflection scenario is much preferred, which is consistent with previous studies. Cackett et al. (2010) analyzed *Suzaku* data of Serpens X-1 and found relativistically-blurred iron emission lines. The recent *NuSTAR* observation (Miller et al. 2013) confirms the presence of the relativistic iron line, together with the Compton hump. In this work, we construct several models to test the relativistic reflection scenario and find that blurred reflection explains the Fe line profile significantly better than single/multiple Gaussian lines. Thanks to the remarkable resolving power of *Chandra* HETGS, the grating spectrum is capable of detecting narrow emission lines. In our analysis, no narrow line components are required, and must be weak if they exist.

The broad iron line profile implies a small inner radius, and we obtain an inner radius of ~7–8 R_G. This sets an upper limit to the NS radius of ~15–17 km (assuming the mass of the NS is ~1.4 $M_\odot$). Furthermore, a low inclination angle of ~25°–35° is found, which is consistent with the previous measurements. We also find that the choice of continuum does not affect the values of the line-related parameters, which further confirms the robustness of the fitting results. We conclude that the Fe emission line observed in the X-ray spectrum of Serpens X-1 is broad and shaped by relativistic effects.
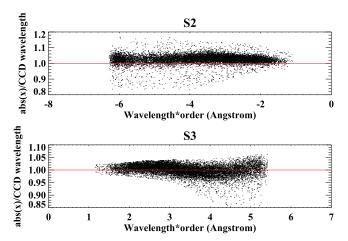

Figure 6. HEG +1 (in black) and −1 (in red) detector effective areas in the upper panel. The lower panel of the figure shows the Serpens X-1 HEG +1 (black data points) and −1 (red data points) data/model ratios. The continuum is modeled as `tbabs*(diskbb + bbody + power-law)`. The plot reveals the poor calibration of the HEG +1 spectrum. The vertical dashed lines are intended to help guide the eye.

APPENDIX
DISCREPANCY BETWEEN THE +1 AND −1 SPECTRA

We aim to analyze data with the maximum signal-to-noise ratio, and so we seek to combine the HEG +1 and −1 spectra. The HEG ±1 spectra are, however, discrepant and not suitable for combination. In Figure 6, we plot the detector effective areas and data/model ratio of the HEG ±1 spectra (+1 in black and −1 in red data points) fitted by a simple continuum `tbabs*(diskbb + bbody + power-law)`. It can been seen that the ±1 spectra disagree in most of the HEG energy band (at the 5%–10% level), although both show similar Fe line profiles when the continuum is properly modeled. The wiggles and emission features shown in the −1 spectrum below 2.0 keV cannot be modeled and match changes in the effective area, and thus are likely due to calibration uncertainties. There are obvious deviations over the 2–5 keV band between the ±1 spectra. It seems that the HEG +1 spectrum suffers calibration problems, while the HEG −1 spectrum does not show unexpected features in the 2–5 keV energy band. The location of the zeroth-order image on the chip determines at which energies the chip gaps lie. Here, a 1 arcmin y-offset was applied on the zeroth order in order to place it in a location to avoid any chip gaps near the Fe K band. This results in a chip gap at around 2.5 keV in the +1 spectrum. The use of such an offset has not been widely reported previously, which may explain the issues here. The ~2.5 keV drop in the +1 spectrum matches with a large change in the effective area due to a chip gap (as marked by dashed lines in Figure 6). Uncertain calibration around this gap clearly leads to the residuals. There also seems to be excess emission around 3–4 keV. This has been a known issue for HETGS data in CC mode, probably caused by

Figure 7. Order-sorting region of chips S2 and S3. The *x*-axis is the wavelength times order, and the *y*-axis the absolute value of *x*-value over the CCD wavelength. The figure shows the selected events during the order-sorting process. The mild curvature shown in S3 might be the cause of discrepancy between the HEG ±1 spectra.

improper order sorting table (OSIP) or charge transfer inefficiency (CTI) corrections.[14]

As opposed to the "time event (TE)" mode, in the CC mode every CCD suffers from time-dependent CTI. The CTI correction relies on charge trap maps for each device to predict charge losses and correct them. Nevertheless, in CC mode, charges are clocked continuously and may lead to time-dependent charge trap maps; each CCD suffers from this effect. Inappropriate CTI correction may cause events to fall outside of the OSIP. So far, alternate trap maps for the CC mode have not been found, but the *Chandra* calibration team provided a few possible methods to solve this issue (see footnote 14). One can primarily use HEG −1 and MEG +1 orders only, or applying a custom OSIP could possibly fix the problem.

We examined the order-sorting regions of each CCD by plotting the grating wavelength (wavelength times order) against the wavelength over the CCD wavelength ($hc/$ENERGY). Only HEG first-order data have been used, and we show the order-sorting regions of chips S2 and S3, where the ~2–5 keV ±1 spectra were extracted, in Figure 7. Ideally, data points should be evenly distributed along the $y = 1$ axis. Most events on chip S2 lie slightly above unity (similar to those on S1, S4, and S5), while the distribution of those on chip S3 shows mild curvatures, which might be the reason that the +1 spectrum is not consistent with the −1 spectrum. One possible way to improve the ±1 spectral agreement is to modify the event file and bring the *y*-value in Figure 7 close to unity. We first tried to correct the ENERGY column in the level = 1.5 (after order sorting) event file by dividing the column by the average *y*-value of each chip and extracting spectra from the corrected event file. We also tried a more sophisticated method, which modifies the ENERGY column node by node, i.e., applying a spline fit to make certain that every event lies on $y = 1$. However, neither of the methods noticeably improved the spectra. We then tried to modify the level = 1 (before order sorting) event file and re-run `tg_resolve_events` to process order sorting on the corrected event file, and extracted a new spectrum from the new event file after order sorting.

---

[14] http://cxc.harvard.edu/cal/Acis/Cal_prods/ccmode/ccmode_final_doc02.pdf

Modifying the level = 1 event file does give different spectra, but it seems to cause problems for order sorting and the spectra are clearly not corrected properly.

Another method for addressing this issue is to widen the order-sorting window. When data are taken under CC mode, the Y position of an event is not known and the order selection can be tricky. In some cases, the spectra can be smoothed out by including events that fell outside of the OSIP. When running `tg_resolve_events`, by setting the script to disable the original OSIP file and indicating the numbers of parameters "osort_hi" and "osort_lo," one can customize the size of the order-sorting window. We set both osort_hi and osort_lo to be 0.2 (including events fell in the regime $0.8 < y < 1.2$ in Figure 7) to widen the event order-sorting window. We find that this does not help to eliminate discrepancies between the ±1 spectra but, on the contrary, makes the issue worse. By widening the order-sorting window, more events are selected, and hence spectra with higher fluxes are created. The 3–4 keV excess emission in the +1 spectrum turned out to be larger than the original spectrum before correction. In this case, widening the order-sorting window does not effectively solve the problem.

We look for a correction that would remove the 3–4 keV excess from the HEG +1 spectrum. As widening the order-sorting would increase the flux of this energy band, narrowing the window might provide the correction that we need. We find that setting osort_hi = 0.2 and osort_lo = 0.04 (including events fell in the regime $0.96 < y < 1.2$) improves the agreement of the ±1 spectra. The corrected +1 spectrum does not completely match the −1 spectrum, but the flux level between 2 and 5 keV is much more similar than the spectrum before correction. Although, unfortunately, it is still not good enough to combine the ±1 spectra and achieve maximum signal-to-noise ratio, we find that applying a SMEDGE component in XSPEC with negative optical depth to the +1 spectrum when fitting significantly improves data agreement over the 2–5 keV energy band. The SMEDGE component can mimic the sharp feature caused by the change in effective area and reduce the residuals. Yet it seems that different continuum models are required to fit the +1 and −1 spectra, and thus we only present results of the −1 spectrum in the paper. Nevertheless, fitting the +1 spectrum including SMEDGE and allowing for a different continuum model than the −1 spectrum results in the same conclusions and consistent parameters for the relativistic iron line.

REFERENCES

Arnaud, K. A. 1996, in ASP Conf. Ser. 101, Astronomical Data Analysis Software and Systems V, ed. G. H. Jacoby, & J. Barnes (San Francisco, CA: ASP), 17
Asai, K., Dotani, T., Nagase, F., & Mitsuda, K. 2000, ApJS, 131, 571
Ballantyne, D. R. 2004, MNRAS, 351, 57
Ballantyne, D. R., Purvis, J. D., Strausbaugh, R. G., & Hickox, R. C. 2012, ApJL, 747, L35
Bardeen, J. M., Press, W. H., & Teukolsky, S. A. 1972, ApJ, 178, 347
Barret, D. 2001, AdSpR, 28, 307
Barret, D., Olive, J. F., Boirin, L., et al. 2000, ApJ, 533, 329
Bhattacharyya, S. 2011, MNRAS, 415, 3247
Bhattacharyya, S., & Strohmayer, T. E. 2007, ApJL, 664, L103
Brenneman, L. W., & Reynolds, C. S. 2006, ApJ, 652, 1028
Brenneman, L. W., Reynolds, C. S., Nowak, M. A., et al. 2011, ApJ, 736, 103
Cackett, E. M., Altamirano, D., Patruno, A., et al. 2009a, ApJL, 694, L21
Cackett, E. M., Miller, J. M., Ballantyne, D. R., et al. 2010, ApJ, 720, 205
Cackett, E. M., Miller, J. M., Bhattacharyya, S., et al. 2008, ApJ, 674, 415
Cackett, E. M., Miller, J. M., Homan, J., et al. 2009b, ApJ, 690, 1847

Cackett, E. M., Miller, J. M., Reis, R. C., Fabian, A. C., & Barret, D. 2012, ApJ, 755, 27
D'Aì, A., di Salvo, T., Ballantyne, D., et al. 2010, A&A, 516, A36
Degenaar, N., Miller, J. M., Chakrabarty, D., et al. 2015, MNRAS, 451, L85
Degenaar, N., Miller, J. M., Harrison, F. A., et al. 2014, ApJL, 796, L9
Di Salvo, T., Iaria, R., Matranga, M., et al. 2015, MNRAS, 449, 2794
Di Salvo, T., Iaria, R., Méndez, M., et al. 2005, ApJL, 623, L121
Dickey, J. M., & Lockman, F. J. 1990, ARA&A, 28, 215
Done, C., Gierliński, M., & Kubota, A. 2007, A&ARv, 15, 1
Done, C., & Zycki, P. T. 1999, MNRAS, 305, 457
Egron, E., Di Salvo, T., Motta, S., et al. 2013, A&A, 550, A5
Fabian, A. C., Iwasawa, K., Reynolds, C. S., & Young, A. J. 2000, PASP, 112, 1145
Fabian, A. C., Nandra, K., Reynolds, C. S., et al. 1995, MNRAS, 277, L11
Fabian, A. C., Rees, M. J., Stella, L., & White, N. E. 1989, MNRAS, 238, 729
Fabian, A. C., Zoghbi, A., Ross, R. R., et al. 2009, Natur, 459, 540
Friedman, H., Byram, E. T., & Chubb, T. A. 1967, Sci, 156, 374
García, J., Dauser, T., Reynolds, C. S., et al. 2013, ApJ, 768, 146
García, J., & Kallman, T. R. 2010, ApJ, 718, 695
George, I. M., & Fabian, A. C. 1991, MNRAS, 249, 352
Hynes, R. I., Charles, P. A., van Zyl, L., et al. 2004, MNRAS, 348, 100
Iaria, R., Lavagetto, G., D'Aí, A., di Salvo, T., & Robba, N. R. 2007, A&A, 463, 289
Inoue, H., & Matsumoto, C. 2003, PASJ, 55, 625
Lamb, D. Q., & Lamb, F. K. 1978, ApJ, 220, 291
Laurent, P., & Titarchuk, L. 2007, ApJ, 656, 1056
Lightman, A. P., & White, T. R. 1988, ApJ, 335, 57
Lin, D., Remillard, R. A., & Homan, J. 2007, ApJ, 667, 1073
Lin, D., Remillard, R. A., & Homan, J. 2010, ApJ, 719, 1350
Lin, D., Remillard, R. A., Homan, J., & Barret, D. 2012, ApJ, 756, 34
Masetti, N., Foschini, L., Palazzi, E., et al. 2004, A&A, 423, 651
Matt, G., Fabian, A. C., & Ross, R. R. 1993, MNRAS, 262, 179
Migliari, S., Fender, R. P., Rupen, M., et al. 2004, MNRAS, 351, 186
Miller, J. M. 2007, ARA&A, 45, 441
Miller, J. M., D'Aì, A., Bautz, M. W., et al. 2010, ApJ, 724, 1441
Miller, J. M., Fabian, A. C., Wijnands, R., et al. 2002, ApJL, 570, L69
Miller, J. M., Maitra, D., Cackett, E. M., Bhattacharyya, S., & Strohmayer, T. E. 2011, ApJL, 731, L7
Miller, J. M., Parker, M. L., Fuerst, F., et al. 2013, ApJL, 779, L2
Miller, J. M., Raymond, J., Fabian, A. C., et al. 2012, ApJL, 759, L6
Misra, R., & Kembhavi, A. K. 1998, ApJ, 499, 205
Misra, R., & Sutaria, F. K. 1999, ApJ, 517, 661
Ng, C., Díaz Trigo, M., Cadolle Bel, M., & Migliari, S. 2010, A&A, 522, A96
Oosterbroek, T., Barret, D., Guainazzi, M., & Ford, E. C. 2001, A&A, 366, 138
Papitto, A., Di Salvo, T., D'Aì, A., et al. 2009, A&A, 493, L39
Pintore, F., Salvo, T. D., Bozzo, E., et al. 2015, MNRAS, 450, 2016
Piraino, S., Santangelo, A., di Salvo, T., et al. 2007, A&A, 471, L17
Piraino, S., Santangelo, A., & Kaaret, P. 2000, A&A, 360, L35
Piraino, S., Santangelo, A., Kaaret, P., et al. 2012, A&A, 542, L27
Reis, R. C., Fabian, A. C., Ross, R. R., & Miller, J. M. 2009, MNRAS, 395, 1257
Reis, R. C., Fabian, A. C., Ross, R. R., et al. 2008, MNRAS, 387, 1489
Reis, R. C., Miller, J. M., Reynolds, M. T., Fabian, A. C., & Walton, D. J. 2012, ApJ, 751, 34
Reynolds, C. S., & Nowak, M. A. 2003, PhR, 377, 389
Reynolds, C. S., & Wilms, J. 2000, ApJ, 533, 821
Ross, R. R., & Fabian, A. C. 1993, MNRAS, 261, 74
Ross, R. R., & Fabian, A. C. 2005, MNRAS, 358, 211
Sanna, A., Hiemstra, B., Méndez, M., et al. 2013, MNRAS, 432, 1144
Seon, K.-I., & Min, K. W. 2002, A&A, 395, 141
Strohmayer, T., & Bildsten, L. 2006, in New Views of Thermonuclear Bursts, ed. W. H. G. Lewin, & M. van der Klis (Cambridge: Cambridge University Press), 113
Tanaka, Y., Nandra, K., Fabian, A. C., et al. 1995, Natur, 375, 659
Vrtilek, S. D., Helfand, D. J., Halpern, J. P., Kahn, S. M., & Seward, F. D. 1986, ApJ, 308, 644
Wilms, J., Allen, A., & McCray, R. 2000, ApJ, 542, 914
Woosley, S. E., & Taam, R. E. 1976, Natur, 263, 101